https://doi.org/10.1016/j.surfcoat.2020.125432



# Novel fabrication of a hierarchical structured surface with improved corrosion inhibition by using hydrothermal synthesis and ultraprecision machining

Yexiang Fu, Zejia Zhao, Waisze Yip, Suet To*

State Key Laboratory of Ultra-precision Machining Technology, Department of Industrial and Systems Engineering, The Hong Kong Polytechnic University, HKSAR, China

**Abstract**

Hydrophobic surfaces are effective on corrosion resistance as the contact with corrosive medium is reduced. In this study, a novel route integrating hydrothermal synthesis with ultraprecision machining (UPM) is reported to prepare a hierarchical cuprous oxide-stearic acid ($Cu_2O$-STA) copper surface. Electrochemical methods were utilized to characterize the corrosion resistance performance. The results indicated that $Cu_2O$-STA surfaces showed good corrosion resistance properties. The enhancement on the properties achieved via introducing UPM fabricated microgrooves was also revealed, by comparing the electrochemical behaviors of $Cu_2O$-STA modified flat samples with the hierarchical surfaces based on $Cu_2O$-STA modified microgrooves.

**Keywords**

Corrosion resistance; Electrochemical characterization; Ultraprecision machining; Hierarchical structures

* Corresponding author.
Email addresses: yexiang.fu@connect.polyu.hk (Y. F.), ze-jia.zhao@connect.polyu.hk (Z. Z.), lennyyip@yahoo.com.hk (W. Y.), sandy.to@polyu.edu.hk (S. T.)

## 1. Introduction

Copper is one of the most important fundamental materials and widely utilized in many industrial fields such as electronics, aviation, automobile and ship building, owing to its superior properties in electrical conductivity, heat transfer, mechanical workability and malleability [1-3]. However, copper is prone to corrosion especially in an aggressive medium, which causes a compromised service lifespan [4]. This poses a threat to the industry economy and has been attracting researchers' interest to work on strategies for an inhibition of corrosion.

As corrosion reactions are triggered by the contact of solid surface and water with aggressive anions, the reduction of the contact area is effective on retarding the corrosion rate. Therefore, fabricating hydrophobic surfaces could be effective on corrosion resistance for engineering materials [5, 6]. Hydrophobicity is governed by two factors: hydrophobic surface chemistry and rough surface structures minimizing wetting area [7-9]. Micro-nanometer scale roughness is expected to enhance hydrophobicity and corrosion resistance, as air can be trapped in the gaps formed by the micro/nano structure, acting as the corrosion inhibitor [10]. Many techniques are applied to prepare such surfaces, as well as the varied methods for characterization and analysis [11-20]. It is noted that most of the fabricated hydrophobic surfaces thus far were based on irregular coatings resulting in roughness and do not possess precise control on dimensions and shapes. Only limited works reported that regularly shaped hydrophobic microstructure was fabricated using milling technique, but it did not provide adequate results to study the underlying mechanism of corrosion resistance associated with surface topography [21]. Hierarchical structures could be fabricated through machining of controlled microstructures followed by modifications with secondary structures and are

effective in increasing hydrophobicity. Hence the corrosion resistance properties are improved [22].

Ultraprecision machining (UPM) is a promising method that provides a feasible solution to the fabrication of micro-patterned surfaces. It is an efficient and flexible way to fabricate high quality surfaces with form accuracy of sub-micrometer and surface roughness up to nanometer range [23]. In a UPM process, a diamond tool could incorporate up to five controlled axes, which provides more degrees of freedom than other mechanical and chemical processes [24, 25]. Therefore, it is applicable for machining a variety of geometries and replicating them into microarrays. There are some typical structures such as micropyramids [26], microgrooves [27], freeform compound-eye microlens array [28] rotational microridges [29] and micro conical array [30], which are utilized in fields including optics, energy and resources. On the other hand, hydrothermal synthesis is an efficient method in creating thin films with micro-nanostructured topography [31, 32]. It is a chemical process performed in an aqueous solution in a sealed vessel above ambient pressure and temperature. The high pressure and temperature facilitate the interactions of the reactants and single crystalline products are obtained [33]. Depending on the precursors and additives, varied micro-nanostructures could be prepared such as nanorods [34], nanospheres [35] and nanoflakes [36].To achieve a hydrophobic surface, the fabrication of metal oxides through hydrothermal synthesis is always followed by treatment of chemicals with low surface energy groups such as fatty acid and fluoroalkyl-silane. This procedure produces a thin layer of organics with low surface energy onto the oxides while retaining the prepared micro-nanostructures [13, 37-40].

This study aims at enhancing the corrosion resistance of copper by applying a new method that integrates UPM with hydrothermal synthesis to fabricate rectangular shaped cuprous oxide on copper plates with machined microgrooves. The shape of the groove gaps could be

precisely controlled in the UPM process. The prepared $Cu_2O$ surface was modified with stearic acid (STA) to achieve a low surface energy. The $Cu_2O$-STA modified with grooved copper was measured through morphological characterization and electrochemical characterization for displaying the corrosion resistance behavior.

## 2. Experimental details

### 2.1 Ultraprecision machining of copper microgrooves

Copper plates used as the substrate were T2 copper (Cu+Ag wt.% over 99.9) purchased from Quanfu Metal Co. (Shenzhen, China). The plates were firstly cut into the dimensions of 10 mm in length, 10 mm in width and 2 mm in thickness. Prior to machining microgroove patterns, rough machining was carried out to obtain a flat copper surface using single-point diamond turning (SPDT) on a Nanoform 200 machine. This ensures that the groove patterns on a large area of sample possess the same size and level. Groove patterns were subsequently fabricated on a Moore Nanotech 350FG ultra-precision freeform generator.

A single crystal diamond cutting tool with specific included angle and width of tool tip was selected to fabricate the microgrooves, as shown in Fig.1(a). The target groove shape was presented in the schematic diagram Fig.1(b) and (c). Trapezoidal grooves with 30 μm in width and 18 μm in depth were fabricated. The angle of the slope was 75°, determined by the included angle of the diamond tool tip. The step of the workpiece along x axis was 60 μm, producing grates of 30 μm in width and forming a 50% theoretical air fraction of the sample surface.

## 2.2 Growth of $Cu_2O$ particles by hydrothermal methods

Copper sulfate and stearic acid were obtained from Alfa Aesar. HCl, NaCl, urea, ethanol and acetone were acquired from Sinopharm. All the reagents were analytical purity and do not need further purification. Pretreatment was taken on flat copper samples as well as the machined copper plates with microgrooves. The flat samples were ground with SiC paper of sequentially finer grit down to 800, and then polished with 0.05 μm polishing paste till mirror-shine. To remove oxide layer from the surface, the copper plates were immersed in 3 wt.% HCl for 20 min. The polished flat samples and the machined groove samples were both washed with copious water, and then ultrasonically cleaned with acetone, ethanol and distilled water in sequence.

The fabrication of rectangular shaped cuprous oxide was carried out as follows. In a typical synthesis, 50 mL solution containing 0.25 g copper sulfate pentahydrate and 0.06 g urea were prepared and stirred uniformly. Then it was transferred to a Teflon-lined autoclave and the copper plate was immersed in it. The autoclave was sealed and heated to 120°C for 6h. After the autoclave was cooled down to room temperature, the copper plate was taken out from the solution and rinsed with copious distilled water. A dark oxide layer could be observed to have formed on the copper plate. After dried in the oven at 80 °C for 2 h, it was immersed in an ethanol solution (2.0 wt.%) of stearic acid (STA) for 2 h at room temperature. Finally, the acquired sample was rinsed with ethanol and then dried in the air. The hierarchical structure was fabricated through the UPM process to acquire microgrooves as the base and subsequent hydrothermal synthesis to prepare $Cu_2O$-STA as the secondary structure.

## 2.3 Surface characterization

The profile of the fabricated microgrooves was observed using a white light interferometer Zygo Nexview. The cross-section view was acquired to show the depths of the groove gaps on different samples. The morphology of $Cu_2O$ layer was examined using a Tescan Vega3 scanning electron microscopy. The phase composition of the crystalline structure of the products was analyzed by X-ray diffraction (XRD) on a Rigaku Smartlab diffractometer equipped with Cu Kα radiation at a scan rate of 5° $min^{-1}$. In all cases, the corrosion experiments were carried out in a 3.5 wt.% aqueous NaCl solution. The anticorrosion behavior of the $Cu_2O$-STA modified copper microgrooves was investigated by the measurements of electrochemical impedance spectra (EIS) and Tafel polarization on a CHI660e electrochemical workstation (Shanghai Chenhua Instrument Co., China). A conventional three-electrode system was used with a saturated Ag/AgCl electrode as the reference electrode and two symmetrically distributed carbon stick electrodes as the counter electrode. The EIS curves were obtained at the open circuit potential using a 10 mV amplitude sinusoidal signal in the frequency range of $10^5$ to $10^{-2}$ Hz. The Tafel curves were obtained at a scan rate of 0.5 mV/s in the range of about ±300 mV vs. open circuit potential.

## 3. Results and discussion

### 3.1 Ultraprecision machining of microgrooves

The fabricated microgrooves are examined using the interferometer and the topography is displayed in Fig. 2. The depth of the grooves is designed to be 18 μm and the top width of grates is 30 μm. The period of the groove structure is 60 μm. From the measured results showing the cross-section view perpendicular to the grooves in Fig. 2(b), the fabricated surface presents good form accuracy. The minor deviations resulted from vibration of the tool and material elastic recovery [41, 42]. Measuring the surface area within a single grate or

groove, the machined surface was smooth with a satisfactory roughness no larger than 0.01 μm. As shown in Fig. 2(c), the surface becomes rough after the modification with $Cu_2O$-STA. Meanwhile, the height of $Cu_2O$-STA groove remains almost the same with that before coating. This indicates that the fabrication of secondary structure has roughly retained the designed shape of the base microgrooves.

3.2 Characterization of hierarchical $Cu_2O$-STA modified microgrooves

To verify the phase and composition of the acquired oxide through hydrothermal synthesis, XRD analysis was performed on the prepared sample. The XRD pattern is shown in Fig. 3. Sharp diffraction peaks around 29˚,37˚, 43˚ and 62˚ are corresponding to planes (110), (111), (200), (220) of $Cu_2O$, which provide a clear evidence for the formation of cuprous oxide. The peaks around 44° and 51° are corresponding to planes (111) and (200) of copper, respectively. The large intensity of Cu peaks is owing to copper as the sample substrate. No side products such as CuO and $Cu(OH)_2$ were detected. The reduction of Cu(II) might be due to the ammonia resolved from urea.

The morphologies of the fabricated $Cu_2O$ were examined by SEM, as shown in Fig. 4. The copper microgrooves fabricated by UPM are displayed in Fig. 4(a). The surface is quite smooth and there are no large defects in groove shape. In Fig. 4(b) and (c), rectangular-shaped $Cu_2O$ particles are formed with an average grain size of about 1 μm. The oxide crystals are distributed uniformly and covered almost the whole surface. The thickness of the film is around 6 μm, which can be roughly evaluated from the cross-section view in Fig. 4(d). The groove shape fully covered with cuprous oxide could also be clearly viewed. The $Cu_2O$ film was chemically modified with stearic acid to improve the hydrophobicity. Sessile Drop method was used to measure the static contact angles of the surfaces. The obtained value was an average measured at 3~5 random positions on the same sample (droplet size 5μL). As

displayed in Fig. 5(a), the contact angle of carefully polished care copper is around 86°±1.0°. For the $Cu_2O$-STA modified copper microgrooves, the contact angle increases to 144°±1.5°, shown in Fig. 5(b). This reflects the hydrophobicity of the fabricated hierarchical structured surface. When immersed in water, hydrophobic surfaces are exceptionally bright when viewed in an oblique angle. The width of a single groove of the hierarchical $Cu_2O$-STA modified microgroove hydrophobic surface is about 30 μm, and therefore it is enabled to be observed through an optical microscope when it is immersed in water, as displayed in Fig. 5(c). The periodically distributed bright lines are air trapped in microgrooves. According to the Laplace-Young equation, a small groove width and a large groove depth are effective on maintaining the air layer [43].

3.3 Corrosion behaviors test of the $Cu_2O$-STA modified copper microgrooves

EIS is a nondestructive technique to characterize the electrochemical reactions and subprocesses occurring at electrode-electrolyte interfaces. It could provide important information regarding the corrosion reaction mechanisms. Fig. 6 shows Nyquist plots and Bode modulus plots of the bare copper, bare copper grooves and the surface modified Cu samples. The EIS data could be analyzed by the ZView2 program with an appropriate equivalent electrical circuit (EEC). As bare metal and metal with a hydrophobic coating were physiochemically different, two circuit models were applied to fit the EIS spectra. The two EEC models are displayed in Fig. 7. In the circuits, $R_s$ is equivalent to the solution resistance and $R_{ct}$ is the charge transfer resistance. $R_{ct}$ is indicative of total corrosion resistance performance. CPE is often used as a substitute for the capacitor in an equivalent circuit to better fit the behavior of electrical double layer. In Fig. 7(b), $R_c$ is introduced due to the existence of the hydrophobic layer. The $R_{ct}/C_{dl}$ elements show the interface reaction on the $Cu_2O$-STA film.

The corrosion resistance could be judged qualitatively from the diameter of the Nyquist semicircles, as shown in Fig. 6(a). In general, an increase of the diameter implies a rise of corrosion resistance. The diameter of the Nyquist loop for $Cu_2O$-STA modified samples is significantly larger than that of a bare copper. For the $Cu_2O$-STA modified grooved copper, it was also larger than that of the modified flat copper. The results indicate that the presented $Cu_2O$-STA layer contributes to good corrosion resistance and that the $Cu_2O$-STA layer on microgrooves presented even better corrosion resistance. This is owning to the hydrophobic oxide layer as the corrosion inhibitor, and the air trapped in the microgrooves further improved the performance, which reduced the contact of the sample and the electrolyte. Bare copper microgrooves are more prone to corrosion according to the EIS spectra as the corrosive medium would penetrate the grooves instead of forming an air layer, which enlarges the contact area of the copper surface and the electrolyte. The fitted data by using ZView2 program are presented in Table I. The $R_{ct}$ of $Cu_2O$-STA modified flat copper was remarkably larger than bare copper, and it became approximately double the value when $Cu_2O$-STA was coated on the microgrooves to form a hierarchical structure. The Bode modulus at the lowest frequency is also used to estimate the corrosion activity. A large impedance modulus is indicative of good anticorrosion capability. As in Fig. 6(b), the Bode plots show an increase of corrosion resistance from the bare copper microgrooves to $Cu_2O$-STA coated on grooved copper.

Tafel plots have been widely used to monitor the instantaneous corrosion rate of metals, alloys and surfaces with coatings, inhibitors or bacteria [44]. In this study, the bare copper and surface-modified copper samples were tested using this technique to evaluate the anticorrosion behaviors. Fig. 8 shows the Tafel plots of the bare copper, bare copper microgrooves, $Cu_2O$-STA modified flat copper and $Cu_2O$-STA modified grooved copper. The

Tafel plots were analyzed by extrapolating the linear anodic and cathodic branches to their intersection to obtain some featuring indexes including corrosion current densities and corrosion potentials. The corrosion current density directly reflects the speed of corrosion reaction. As stated in Table II, for the $Cu_2O$-STA modified flat sample, the corrosion current density is 0.629±0.214 $\mu A \cdot cm^{-2}$, showing a decrease from 1.85±0.57 $\mu A \cdot cm^{-2}$ for the bare Cu. This confirms the anticorrosion property of the $Cu_2O$-STA modification layer. The $Cu_2O$-STA modified microgrooves shows an even smaller corrosion current of 0.176±0.044 $\mu A \cdot cm^{-2}$, which is reduced more than half of the modified flat sample. The results are in good consistence with the EIS spectra, showing good corrosion resistance of the $Cu_2O$-STA layer and the enhancement of the hierarchical structure. The air trapped in grooves reduced the electroactive area of the samples and thus the corrosion current. With the development of hydrophobic surfaces, the samples with large contact angles present a large $R_{ct}$ and decrease in corrosion current, which means good corrosion resistance performance. This improvement in corrosion resistance also benefits from the formation of $Cu_2O$-STA modification layer. In contrast with a laser-textured sample that transits to a superhydrophobic surface in ambient atmosphere [15], this work reveals an overall effect instead of the isolated influence of wettability on corrosion resistance.

## 4. Conclusions

$Cu_2O$-STA modified hierarchical hydrophobic structures were fabricated on copper by combining UPM with hydrothermal synthesis for its corrosion resistance. Rectangular shaped cuprous oxide particles were fabricated on precisely controlled microgrooves. According to the electrochemical measurements, the hydrophobic $Cu_2O$-STA film showed good corrosion resistance. The geometries could be controlled through the UPM process to better form an air

layer as the corrosion inhibitor, and simultaneously, the rough cuprous oxide layer is successfully formed on the microgroove surface. The method proposed in this study provides a feasible option to fabricate hydrophobic anticorrosion surface and systematically investigate the topography influence on corrosion resistance.

**Acknowledgements**

The work described in this paper was partially supported by a grant from the National Natural Science Foundation of China (Project No.: 51675455), General Research Fund from the Research Grants Council of Hong Kong Special Administrative Region under the project code PolyU 152021/17E, and the Research Committee of The Hong Kong Polytechnic University (Project Code: RUNP).

**Author contributions**

Y.F. and S.T. conceptualized this work. Y.F. and Z.Z. undertook device fabrication. Y.F. and W.Y. performed the morphological characterization. Y.F. performed electrochemical experiments presented in this manuscript and analyzed the data. Y.F. prepared the first version of the manuscript. All authors reviewed it and contributed to the final version.

**Competing interests**

The authors declare no competing interests.

**References**

[1] T. Liu, S. Chen, S. Cheng, J. Tian, X. Chang, Y. Yin, Corrosion behavior of super-hydrophobic surface on copper in seawater, Electrochim. Acta, 52 (2007) 8003-8007.

[2] Y. Liu, S. Li, J. Zhang, J. Liu, Z. Han, L. Ren, Corrosion inhibition of biomimetic super-hydrophobic electrodeposition coatings on copper substrate, Corrosion Sci., 94 (2015) 190-196.

[3] M. Može, M. Zupančič, M. Hočevar, I. Golobič, P. Gregorčič, Surface chemistry and morphology transition induced by critical heat flux incipience on laser-textured copper surfaces, Applied Surface Science, (2019).

[4] F. Sinapi, S. Julien, D. Auguste, L. Hevesi, J. Delhalle, Z. Mekhalif, Monolayers and mixed-layers on copper towards corrosion protection, Electrochim. Acta, 53 (2008) 4228-4238.

[5] Y. Huang, D.K. Sarkar, D. Gallant, X.-G. Chen, Corrosion resistance properties of superhydrophobic copper surfaces fabricated by one-step electrochemical modification process, Appl. Surf. Sci., 282 (2013) 689-694.

[6] P. Wang, D. Zhang, R. Qiu, Liquid/solid contact mode of super-hydrophobic film in aqueous solution and its effect on corrosion resistance, Corrosion Sci., 54 (2012) 77-84.

[7] J.-M. Lim, G.-R. Yi, J.H. Moon, C.-J. Heo, S.-M. Yang, Superhydrophobic films of electrospun fibers with multiple-scale surface morphology, Langmuir, 23 (2007) 7981-7989.

[8] N. Verplanck, Y. Coffinier, V. Thomy, R. Boukherroub, Wettability switching techniques on superhydrophobic surfaces, Nanoscale Res. Lett., 2 (2007) 577.

[9] A. Marmur, Hydro-hygro-oleo-omni-phobic? Terminology of wettability classification, Soft Matter, 8 (2012) 6867-6870.

[10] A.M.A. Mohamed, A.M. Abdullah, N.A. Younan, Corrosion behavior of superhydrophobic surfaces: A review, Arab. J. Chem., 8 (2015) 749-765.

[11] Y. Wan, M. Chen, W. Liu, X. Shen, Y. Min, Q. Xu, The research on preparation of superhydrophobic surfaces of pure copper by hydrothermal method and its corrosion resistance, Electrochim. Acta, 270 (2018) 310-318.

[12] Z. Zhang, B. Ge, X. Men, Y. Li, Mechanically durable, superhydrophobic coatings prepared by duallayer method for anti-corrosion and self-cleaning, Colloid Surf. A-Physicochem. Eng. Asp., 490 (2016) 182-188.

[13] Y. Fan, Z. Chen, J. Liang, Y. Wang, H. Chen, Preparation of superhydrophobic films on copper substrate for corrosion protection, Surf. Coat. Technol., 244 (2014) 1-8.

[14] K.A. Emelyanenko, N.A. Sanzharovsky, E.V. Chulkova, A.A. Ganne, A.M. Emelyanenko, L.B. Boinovich, Superhydrophobic corrosion resistant coatings for copper via IR nanosecond laser processing, Mater. Res. Express, 5 (2018) 115001.

[15] U. Trdan, M. Hočevar, P. Gregorčič, Transition from superhydrophilic to superhydrophobic state of laser textured stainless steel surface and its effect on corrosion resistance, Corrosion Sci., 123 (2017) 21-26.

[16] A.-M. Kietzig, S.G. Hatzikiriakos, P. Englezos, Patterned superhydrophobic metallic surfaces, Langmuir, 25 (2009) 4821-4827.

[17] P. Gregorčič, M. Conradi, L. Hribar, M. Hočevar, Long-term influence of laser-processing parameters on (super) hydrophobicity development and stability of stainless-steel surfaces, Materials, 11 (2018) 2240.

[18] P. Gregorčič, B. Šetina-Batič, M. Hočevar, Controlling the stainless steel surface wettability by nanosecond direct laser texturing at high fluences, Appl. Phys. A, 123 (2017) 766.

[19] A.-M. Kietzig, M. Negar Mirvakili, S. Kamal, P. Englezos, S.G. Hatzikiriakos, Laser-patterned super-hydrophobic pure metallic substrates: Cassie to Wenzel wetting transitions, J. Adhes. Sci. Technol., 25 (2011) 2789-2809.

[20] D.V. Ta, A. Dunn, T.J. Wasley, R.W. Kay, J. Stringer, P.J. Smith, C. Connaughton, J.D. Shephard, Nanosecond laser textured superhydrophobic metallic surfaces and their chemical sensing applications, Applied Surface Science, 357 (2015) 248-254.

[21] J. Zhu, X. Hu, A new route for fabrication of the corrosion-resistant superhydrophobic surface by milling process, J. Coat. Technol. Res., (2018).

[22] C. Lee, C.-H. Choi, C.-J. Kim, Superhydrophobic drag reduction in laminar flows: a critical review, Exp. Fluids, 57 (2016) 176.

[23] Z. Zhang, J. Yan, T. Kuriyagawa, Manufacturing technologies toward extreme precision, International Journal of Extreme Manufacturing, (2019).

[24] M.A. Davies, C.J. Evans, R.R. Vohra, B.C. Bergner, S.R. Patterson, Application of precision diamond machining to the manufacture of microphotonics components, SPIE, 2003.

[25] S. Zhang, Y. Zhou, H. Zhang, Z. Xiong, S. To, Advances in ultra-precision machining of microstructured functional surfaces and their typical applications, Int. J. Mach. Tools Manuf., 142 (2019) 16-41.

[26] S. Ge, W. Liu, S. Zhou, S. Li, X. Sun, Y. Huang, P. Yang, J. Zhang, D. Lin, Design and preparation of a micro-pyramid structured thin film for broadband infrared antireflection, Coatings, 8 (2018) 192.

[27] C.T. Cheng, G. Zhang, S. To, Wetting characteristics of bare micro-patterned cyclic olefin copolymer surfaces fabricated by ultra-precision raster milling, RSC advances, 6 (2016) 1562-1570.

[28] L. Li, Y.Y. Allen, Design and fabrication of a freeform microlens array for a compact large-field-ofview compound-eye camera, Appl. Optics, 51 (2012) 1843-1852.

[29] L. Li, Y.Y. Allen, Design and fabrication of a freeform microlens array for uniform beam shaping, Microsyst. Technol., 17 (2011) 1713-1720.

[30] B.T.W. Ang, J. Zhang, G.J. Lin, H. Wang, W.S.V. Lee, J. Xue, Enhancing Water Harvesting through the Cascading Effect, ACS Appl. Mater. Interfaces, 11 (2019) 27464-27469.

[31] Q. Zhang, K. Zhang, D. Xu, G. Yang, H. Huang, F. Nie, C. Liu, S. Yang, CuO nanostructures: synthesis, characterization, growth mechanisms, fundamental properties, and applications, Prog. Mater. Sci., 60 (2014) 208-337.

[32] S.S. Mali, C.A. Betty, P.N. Bhosale, P.S. Patil, C.K. Hong, From nanocorals to nanorods to nanoflowers nanoarchitecture for efficient dye-sensitized solar cells at relatively low film thickness: All Hydrothermal Process, Sci. Rep., 4 (2014) 5451.

[33] A.V. Nikam, B.L.V. Prasad, A.A. Kulkarni, Wet chemical synthesis of metal oxide nanoparticles: a review, CrystEngComm, 20 (2018) 5091-5107.

[34] N.S. Ridhuan, K.A. Razak, Z. Lockman, Fabrication and Characterization of Glucose Biosensors by Using Hydrothermally Grown ZnO Nanorods, Sci. Rep., 8 (2018) 13722.

[35] P. Ou, Q. Zhou, J. Li, W. Chen, J. Huang, L. Yang, J. Liao, M. Sheng, Facile ethylene glycol-assisted hydrothermal synthesis of MoO2 nanospheres for high–performance supercapacitors, Mater. Res. Express, 6 (2019) 095044.

[36] K. Thirumalai, M. Shanthi, M. Swaminathan, Ho2WO6/ZnO nanoflakes for photo–electrochemical and self cleaning applications, Mater. Sci. Semicond. Process., 90 (2019) 78-86.

[37] B. Chantal, P. Thierry, T. Mireille, L. Daniel, A ZnO nanowire array film with stable highly waterrepellent properties, Nanotechnology, 18 (2007) 365705.

[38] F. Xiao, S. Yuan, B. Liang, G. Li, S.O. Pehkonen, T. Zhang, Superhydrophobic CuO nanoneedlecovered copper surfaces for anticorrosion, J. Mater. Chem. A, 3 (2015) 4374-4388.

[39] J. Long, M. Zhong, P. Fan, D. Gong, H. Zhang, Wettability conversion of ultrafast laser structured copper surface, J. Laser Appl., 27 (2015) S29107.

[40] J. Long, M. Zhong, H. Zhang, P. Fan, Superhydrophilicity to superhydrophobicity transition of picosecond laser microstructured aluminum in ambient air, J. Colloid Interface Sci., 441 (2015) 1-9.

[41] J. Guo, J. Zhang, H. Wang, K. Liu, A.S. Kumar, Surface quality characterisation of diamond cut V-groove structures made of rapidly solidified aluminium RSA-905, Precision Engineering, 53 (2018) 120-133.

[42] X. Zhang, D. Hui, K. Liu, H. Wang, Effect of air blow pressure in ultrasonic vibration cutting of steel using PCD tools, Proceedings of the 17th International Conference of the European Society for Precision Engineering and Nanotechnology, EUSPEN 2017, 123 - 124

[43] C.-H. Choi, U. Ulmanella, J. Kim, C.-M. Ho, C.-J. Kim, Effective slip and friction reduction in nanograted superhydrophobic microchannels, Phys. Fluids, 18 (2006) 087105.

[44] G.P. Shumakovich, G.V. Otrokhov, M.E. Khlupova, I.S. Vasil'eva, E.A. Zaitseva, O.V. Morozova, A.I. Yaropolov, Laccase-catalyzed synthesis of aniline oligomers and their application for the protection of copper against corrosion, RSC Adv., 4 (2014) 30193-30196.

Table I Fitted parameters of EIS spectra

| Samples | $R_s$ ($\Omega \cdot cm^2$) | CPE ($\mu F \cdot cm^{-2}$) | $R_c$ ($\Omega \cdot cm^2$) | $C_{dl}$ ($\mu F \cdot cm^{-2}$) | $R_{ct}$ ($\Omega \cdot cm^2$) |
|---|---|---|---|---|---|
| Bare copper | 8.32±0.81 | 26.2±3.2 | - | - | $5.79\times10^3\pm4.32\times10^2$ |
| Bare copper microgrooves | 9.35±1.36 | 0.91±0.16 | - | - | $4.30\times10^3\pm4.24\times10^2$ |
| $Cu_2O$-STA on flat copper | 40.4±8.6 | 1.06±0.28 | $3.14\times10^4\pm6.24\times10^3$ | 1.05±0.49 | $6.89\times10^5\pm1.95\times10^5$ |
| $Cu_2O$-STA on grooved copper | 605±101 | 1.13±0.32 | $3.78\times10^5\pm8.61\times10^4$ | 1.81±0.39 | $1.56\times10^6\pm1.96\times10^5$ |

Table II Electrochemical parameters from polarization curves of different samples

| Samples | $E_{corr}$/V | $I_{corr}$/μA·cm$^{-2}$ |
|---|---|---|
| Bare copper | -0.215±0.022 | 1.85±0.57 |
| Bare copper microgrooves | -0.195±0.006 | 4.33±0.88 |
| $Cu_2O$-STA on flat copper | -0.048±0.004 | 0.629±0.214 |
| $Cu_2O$-STA on grooved copper | -0.073±0.019 | 0.176±0.044 |

Fig.1 (a) the tip of the diamond tool under an optical microscope, (b) the schematic diagram of microgrooves surface generation and (c) the cross-section view of the trapezoidal grooves

Fig. 2 Surface profile acquired by the interferometer. (a) The 3D plot of the copper microgrooves, (b) cross-section view perpendicular to the groove direction of copper microgrooves and (c) cross-section view of microgrooves after coated with cuprous oxide.

Fig. 3 XRD of prepared $Cu_2O$ film on copper substrate

Fig. 4 SEM images of (a) copper microgrooves fabricated by UPM, $Cu_2O$-STA film on (b) flat copper plate, (c) copper microgrooves and (d) the cross-section view of $Cu_2O$-STA film

Fig. 5 The contact angles of (a) flat copper plate and (b) $Cu_2O$-STA film on copper microgrooves and (c) the air layer of $Cu_2O$-STA film on copper microgrooves immersed in water

Fig. 6 Nyquist (a) and Bode (b) plots of the bare Cu, $Cu_2O$-STA modified flat copper and $Cu_2O$-STA modified grooved copper. The inset of Nyquist plots is the amplification of the high frequency part

Fig. 7 The equivalent electric circuits for modeling the EIS spectra of (a) bare copper, bare copper microgrooves, (b) the $Cu_2O$-STA modified flat copper and grooved copper with 3.5 wt.% NaCl solution as the electrolyte

Fig. 8 Potentiodynamic polarization curves in 3.5 wt.% NaCl solution.

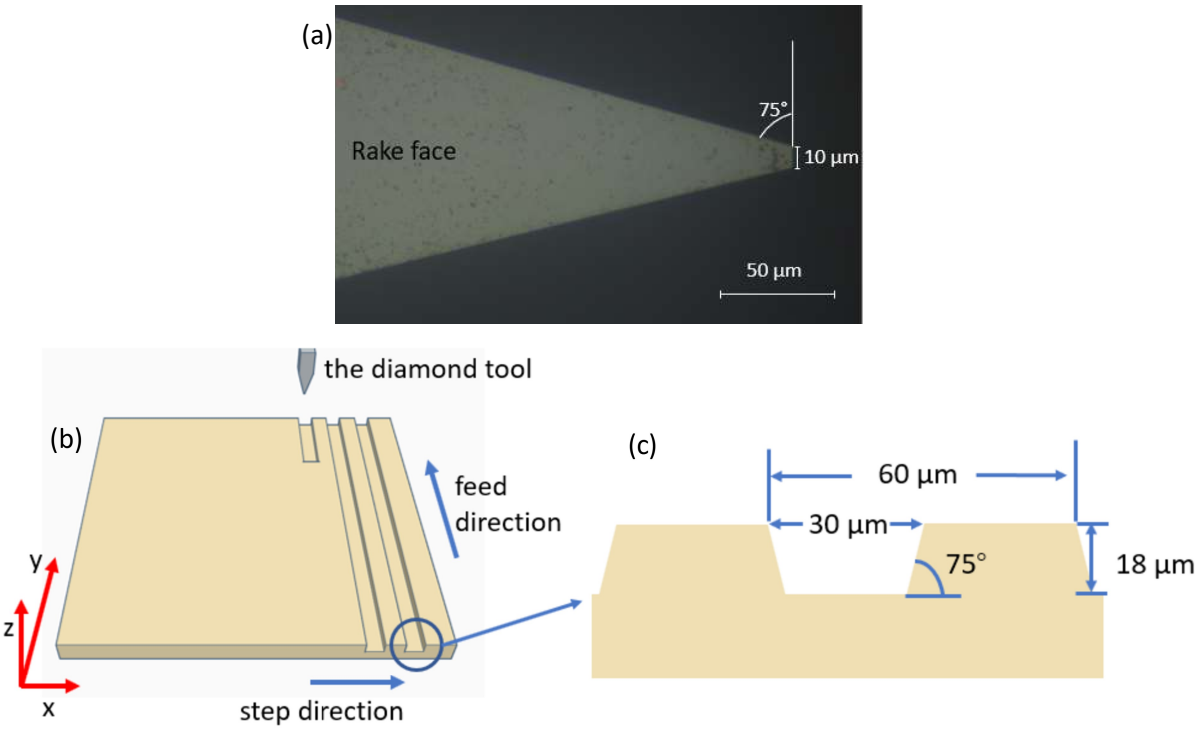


Fig.1

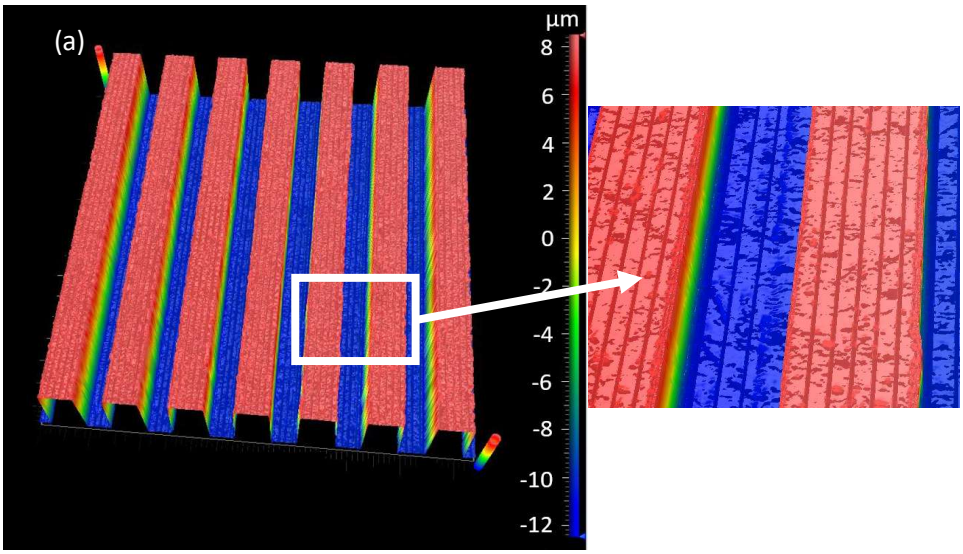
(a)
μm
8
6
4
2
0
-2
-4
-6
-8
-10
-12

(b)

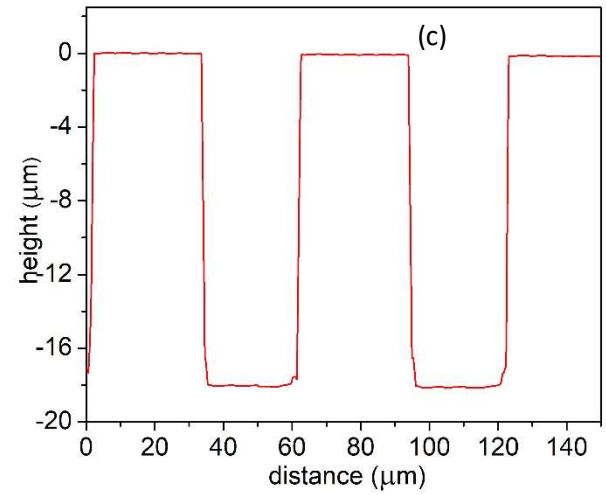
(c)
height (μm)
0
-4
-8
-12
-16
-20
0
20
40
60
80
100
120
140
distance (μm)

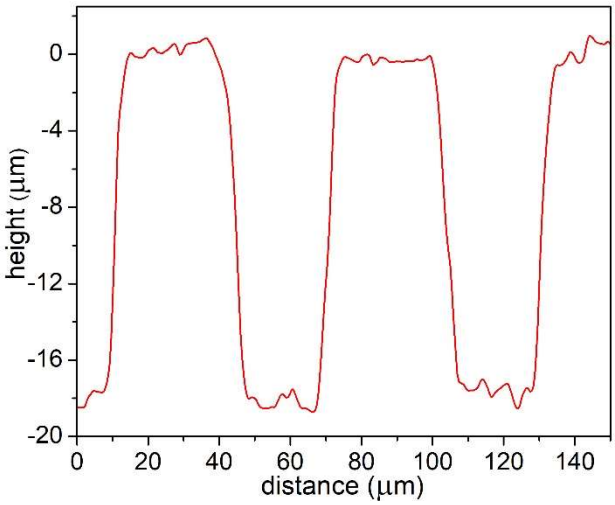
height (μm)
0
-4
-8
-12
-16
-20
0
20
40
60
80
100
120
140
distance (μm)

Fig. 2

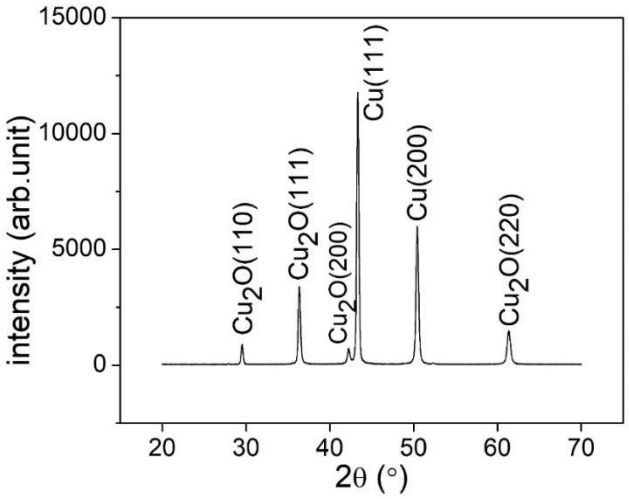


Fig. 3

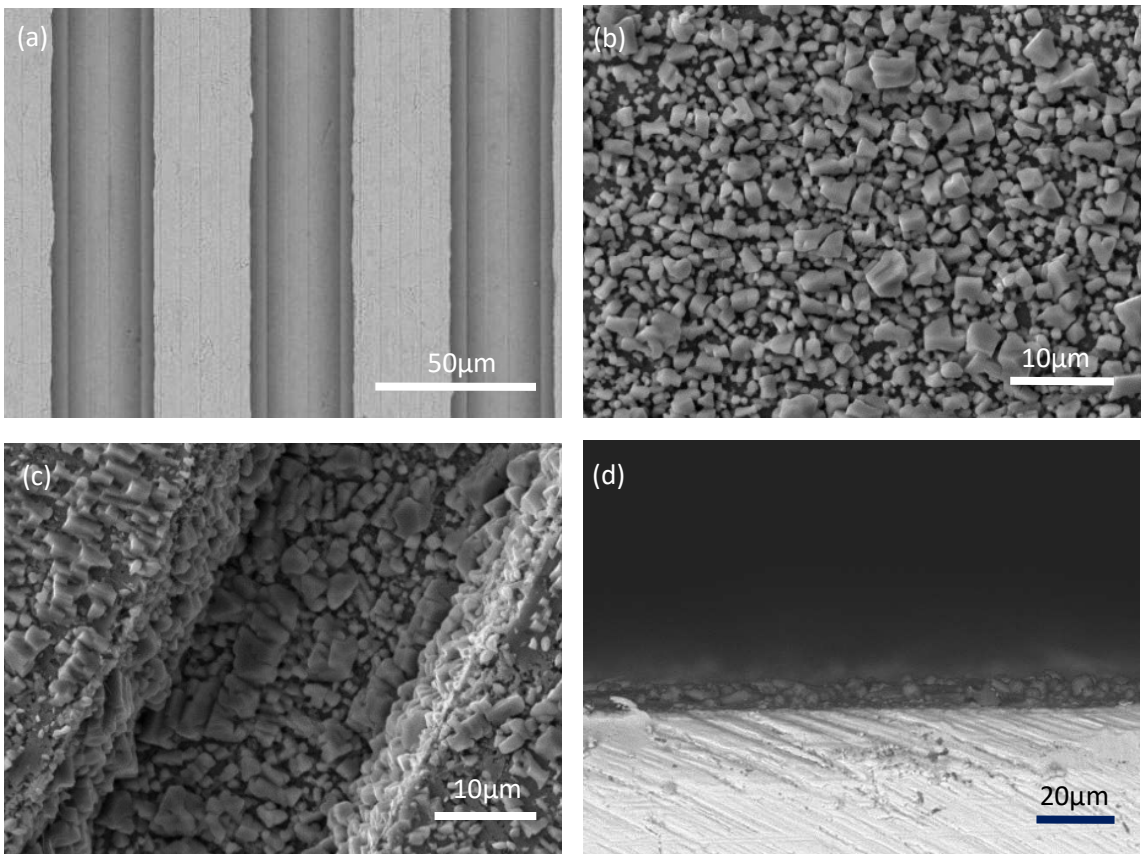


Fig. 4

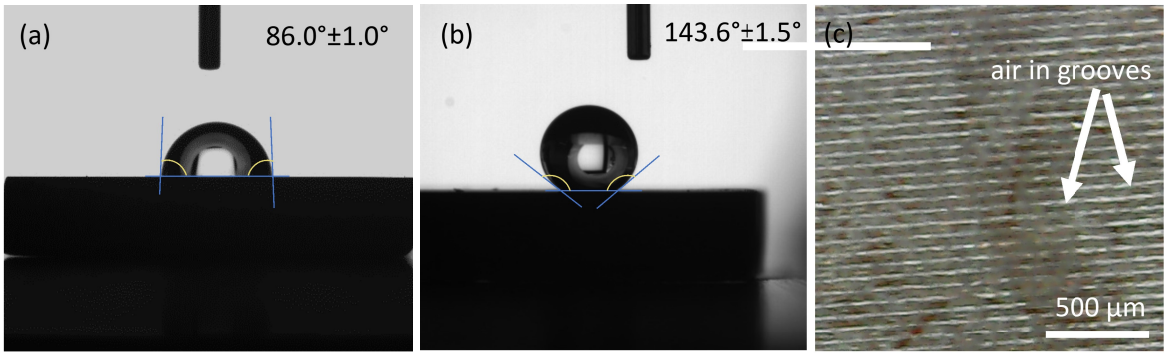
(a)
86.0°±1.0°
(b)
143.6°±1.5°
(c)
air in grooves
500 µm

Fig. 5

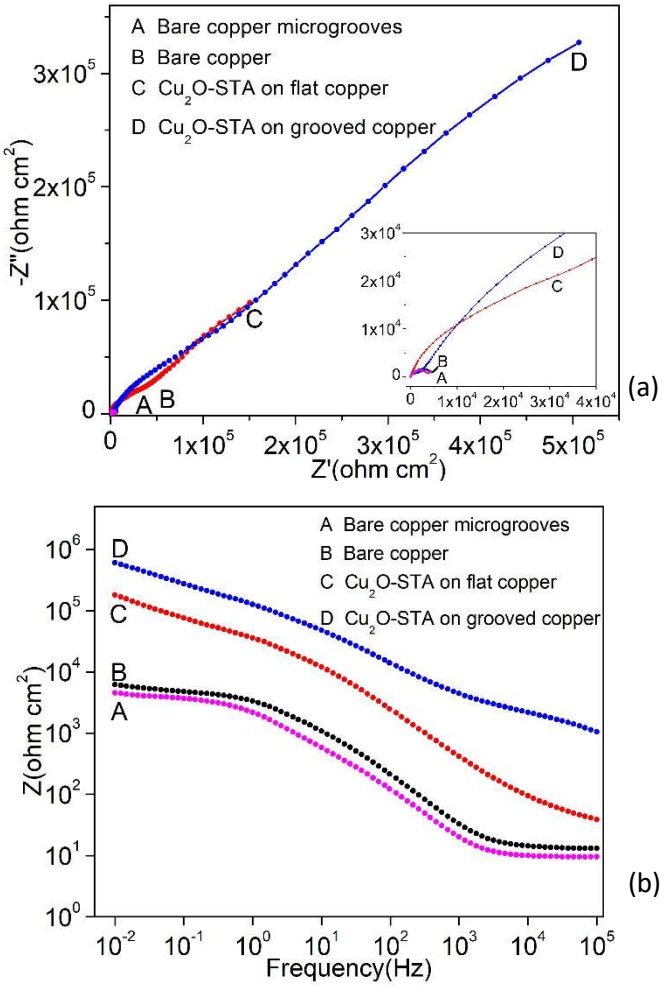
A Bare copper microgrooves
B Bare copper
C Cu2O-STA on flat copper
D Cu2O-STA on grooved copper
-Z''(ohm cm2)
Z'(ohm cm2)
(a)
Z(ohm cm2)
Frequency(Hz)
(b)

Fig. 6

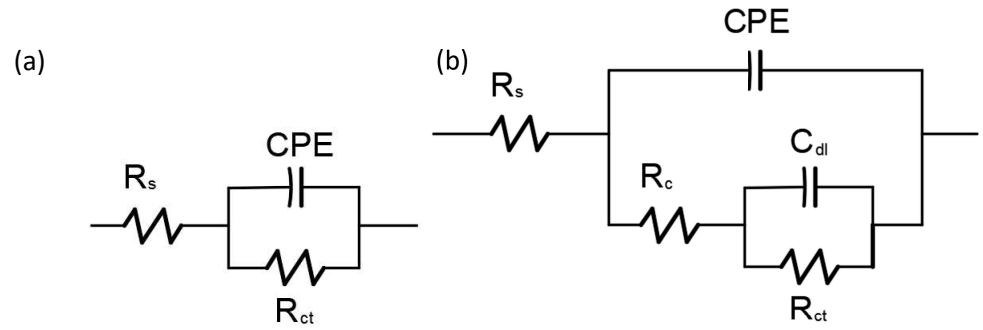
(a)
CPE
Rs
Rct
(b)
CPE
Rs
Cdl
Rc
Rct

Fig. 7

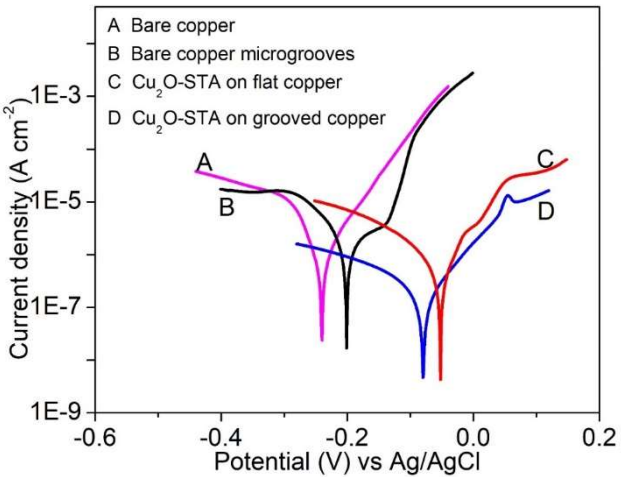
A Bare copper
B Bare copper microgrooves
C Cu2O-STA on flat copper
D Cu2O-STA on grooved copper
Current density (A cm-2)
1E-3
1E-5
1E-7
1E-9
-0.6
-0.4
-0.2
0.0
0.2
Potential (V) vs Ag/AgCl
A
B
C
D

Fig. 8